# Multifunctional Laser-Induced Bubble Micro-Resonator for Upconversion Emission Enhancement

*Monika Kataria, Catherine Currie Duncan, Bergen Polinko Murray, Manav Bindesh Parikh, Zijie Yan**

Department of Applied Physical Sciences, University of North Carolina at Chapel Hill, Chapel Hill, North Carolina 27599, United States

*Corresponding author: Zijie Yan zijieyan@unc.edu

**ABSTRACT:** Lanthanide-doped upconversion nanoparticles (UCNPs) are attractive luminescent materials for nanophotonic applications under near-infrared excitation, but their full potential is still limited by the low quantum yield of upconversion emission. Herein, we have designed and demonstrated a strategy to enhance the emission of a UCNPs film by a laser-induced microbubble. The microbubble plays multifunctional roles, including collecting plasmonic Ag NPs from the solution by the Marangoni convention, printing them on the UCNPs film to enhance the emission by localized surface plasmon resonances, and serving as a bubble micro-resonator to enable optical whispering gallery modes (WGMs). Together, the bubble micro-resonator along with plasmonic Ag NPs can enhance the upconversion emissions by over 200 times. This integrated approach opens new pathways for simultaneous enhancement of emissions from luminescent materials and assembly of NPs over desirable surfaces for optomechanical, biochemical, and sensing applications.

**KEYWORDS:** *upconversion nanoparticles; optical whispering gallery modes; surface plasmon resonance; bubble-pen lithography; micro-resonator*

## Introduction

The importance and versatility of UCNPs have been proven in various applications ranging from displays,[1] bio-imaging,[2] sensing,[3] optoelectronics,[4, 5] photovoltaics,[6] photocatalysis,[7, 8] therapeutics,[9, 10] and diagnostics.[11] UCNPs can exhibit anti-stokes emissions under near infrared (NIR) excitation.[12-15] They are capable of emitting ultraviolet and visible photons by absorbing multiple NIR photons due to their multi-energy level or ladder-like energy level systems.[4, 5] However, the quantum yield of the upconversion emission is generally low due to the multiphoton processes and low absorption cross-section, which hinders the applications of UCNPs.

There are multiple pathways to improve upconversion emissions from the UCNPs under lower excitation intensities. For example, UCNPs can be engineered into multi-core shell nanostructures, where activators (such as $Tm^{3+}$, $Eu^{3+}$, $Er^{3+}$, *etc.*), and sensitizers (such as $Yb^{3+}$) are doped into the host lattices (such as $NaYF_4$) to improve the upconversion emissions. Having an inert shell such as $SiO_2$ or $NaYF_4$ over UCNPs passivates the surface and decrease quenching of upconverting emissions.[16] Integrating UCNPs with plasmonic metal nanostructures and dielectric photonic micro/nano-systems, have led to many-fold upconversion emission enhancements.[17, 18] Based on the localized surface plasmon resonances of metal nanostructures, photons are confined to the ultra-small mode volumes with high photonic density of states. This leads to larger absorption cross-sections.[19] These plasmonic nanostructures can be formed either by self-assembly of metal NPs or lithography techniques such as E-beam lithography, photolithography, *etc.*[20] Quite recently, Chen *et al.* reported 5 times enhancement of upconversion emissions from a tilted plasmonic nanocavity where a single UCNP is placed in the nanogap between a Ag nanocube and a Ag plate.[21] However, the plasmonic hotspot formation is limited to small areas and similar results are difficult to produce at larger scales. This limitation can be overcome by integrating UCNPs

and plasmonic metallic NPs together to dielectric photonic micro-resonators such as polystyrene beads, $SiO_2$ microspheres, microrods, *etc.* Such microspheres can support optical whispering gallery modes (WGMs), as these allow for total internal reflection and trapping of photons thereby amplifying the intensity of the emission from nanomaterials.[22] Recently, Yan *et al.* developed a highly refractive microsphere photonic super-lens array integrated with a flexible UCNP-embedded film which enhanced the upconversion emissions by $10^4$-fold in an all-dielectric microstructure.[23] This enhancement was attributed to optical WGMs, Mie-resonant nano-focusing, and directional antenna effect. These reports highlight the role of UCNPs in dry environments suitable for photonic applications. Like microspheres, the laser induced microbubbles can also enhance emissions from luminescent materials.[24] Integration of luminescent materials and microbubbles in solution would allow for optical imaging or biosensing.[25, 26] However, the challenge lies in developing techniques and methods to create, control, and manipulate micro-bubbles at a solid-liquid interface for real-time applications.

Herein, we have developed a novel platform for enhancing the upconversion emissions from a UCNP film by plasmonic metal NPs and a bubble micro-resonator. The laser-induced bubble is used to create a micro-resonator over a bilayer film of poly(methyl methacrylate) (PMMA) and UCNPs, where Ag NPs are collected at the interface of the microbubble and the PMMA/UCNP film. This platform provides upconversion emissions enhancement by the resonant plasmonic Ag NPs along with the optical WGMs offered by the bubble micro-resonator, which enhances the emissions from the UCNPs by over 200 times in comparison to only UCNP. In addition, the growth and gradual disintegration of the bubble imprints the Ag NPs onto the PMMA/UCNP film, which can serve as the bubble-pen lithography[27] for obtaining patterns of metallic NPs over the UCNP film. The multiple roles of microbubbles are suitable for making multifunctional devices to fulfil

the present sustainable technological needs. This work promotes interdisciplinary research based on laser-induced microbubbles and highlights the potential of microbubbles for photonics and biomedical applications.[28-31]

## Methods

**Materials Synthesis.** The lanthanides doped UCNP having a composition of $NaYF_4$: 30% Yb, 1% Tm@$SiO_2$ were synthesized using thermal decomposition method.[32] The synthesis process is discussed in the Supporting Information S1. The Ag NPs with plasmonic resonance around 450 nm were purchased from nanoComposix.

**Materials Characterizations.** A Thermo Scientific™ Talos F200X scanning/transmission electron microscope (S/TEM) was used for to scan the UCNP for TEM images and high-angle annular dark-field (HAADF) imaging of UCNPs with elemental mapping of constituents' elements. A FEI Helios 600 Nanolab Dual Beam SEM was used to scan the size of Ag NPs. A VWR UV-1600PC UV/VIS spectrometer was used for recording the extinction spectra of the UCNPs. An Andor Kymera 328i imaging spectrograph equipped with Newton DU920P CCD was used for recording the upconversion emissions from the sample cell placed on an inverted optical microscope (Olympus IX73). An FLIR Oryx CMOS Camera was used for taking the optical images. A 980 nm diode-pumped solid-state laser was used as the excitation source for UCNPs to record upconversion emissions. A 800 nm continuous wave Ti:Sapphire laser (Spectra-Physics Matisse 2) was used to create photothermal effects at the sample cell surface and obtain microbubbles. The trapping beam was tightly focused by an objective lens (60X, NA=1.2) to an inner surface (*e.g.*, a UCNP/PMMA bilayer coated on a coverslip) of the sample cell, which enabled optical trapping of NPs from the solution. The excitation laser was focused to the back

aperture of the objective, which created an extended optical field to excite a large area of the UCNPs.

**Sample Preparation.** Five different types of sample cells were prepared to study the formation of bubble micro-resonator and its ability to enhance upconversion emissions. The details of the sample cells and their constituents are listed in TABLE 1. In each experiment, a sample cell was fabricated by attaching a coverslip to a silicone spacer with a hole of 5 mm diameter. The thickness of the spacer is 130 μm. The hole was filled with solution or left empty and sealed by another coverslip coated with a designed film. The optical path of the laser is through the cavity and is focused on the top glass coverslip with the film. The UCNPs were dispersed in ethanol, Ag NPs were dispersed in DI water and ethylene glycol, and PMMA was diluted with toluene. The films of UCNPs and PMMA were obtained by spin-coating method where the optimal thickness of UCNPs is about 200 nm, PMMA is ~10 nm, and Ag NPs film is about 150 nm.

TABLE 1. Sample cells and their constituents.

| Sample | Film Constituents | Solution Constituents |
|---|---|---|
| SC1 | None | UCNPs & Ag NPs in ethanol & water mixture (1:1) |
| SC2 | UCNPs/PMMA | Ag NPs in ethylene glycol & water mixture (1:1) |
| SC3 | UCNPs | None |
| SC4 | UCNPs/Ag NPs | None |
| SC5 | UCNPs/ PMMA/Ag NPs | None |

**Simulations.** The Lumerical Finite Difference Time Domain (FDTD) software was used to simulate the luminescence and local electromagnetic field enhancement. To model the radiation characteristics of the upconversion emitting layer, a dipole source was placed at the emitter position. A box monitor was placed around the dipole with a mesh size of 2.5 nm for accurate results. The box monitor was placed such that it could measure the amount of power emitted by the dipole, the power absorbed by the surrounding Ag NPs and the bubble, and the power emitted

to the far field. The radiative decay was calculated based on a reported method.[33, 34] In the FDTD simulation model, a dipole source is located at 15 nm below a PMMA layer of 10 nm thickness. A glass substrate is at 200 nm below the PMMA layer, and a 70 nm diameter Ag NP is on the PMMA layer right above the dipole source. The dipole is in an air environment and the Ag NP is in water. For the simulation with a bubble, the bubble diameter is 600 nm, and we assume the Ag NP is wrapped in a water layer.

**Results & Discussions**

To achieve the bubble micro-resonator, an optical setup was assembled constituting of an optical trapping system working at $\lambda = 800$ nm, an upconversion excitation laser at $\lambda = 980$ nm, an optical microscope, and a spectrometer as shown in Figure 1a. Figure 1b shows the TEM image of the UCNPs ($NaYF_4$: 30 % Yb, 1 % Tm @ $SiO_2$). The UCNPs are monodispersed with average particle diameter size of 24.7 ± 1.8 nm (Figure S1) and hexagonal-β phase $NaYF_4$ crystal structure (Figure S2).[32] The elemental composition and detailed characterization of the UCNPs is discussed in Supporting Information SII. The UCNPs were dispersed in ethanol and exhibited multimodal upconversion emissions around 449 nm and 475 nm under 980 nm excitation as shown in Figure 1c. The Ag NPs of size 70 nm (Figure S4) offered maximum extinction around 450 nm (Figure 1c).[35] The surface plasmonic resonance of these Ag NPs overlaps well with the emissions from the UCNPs upon 980 nm excitation, which offered a suitable platform for enhancing the emissions from the UCNPs.

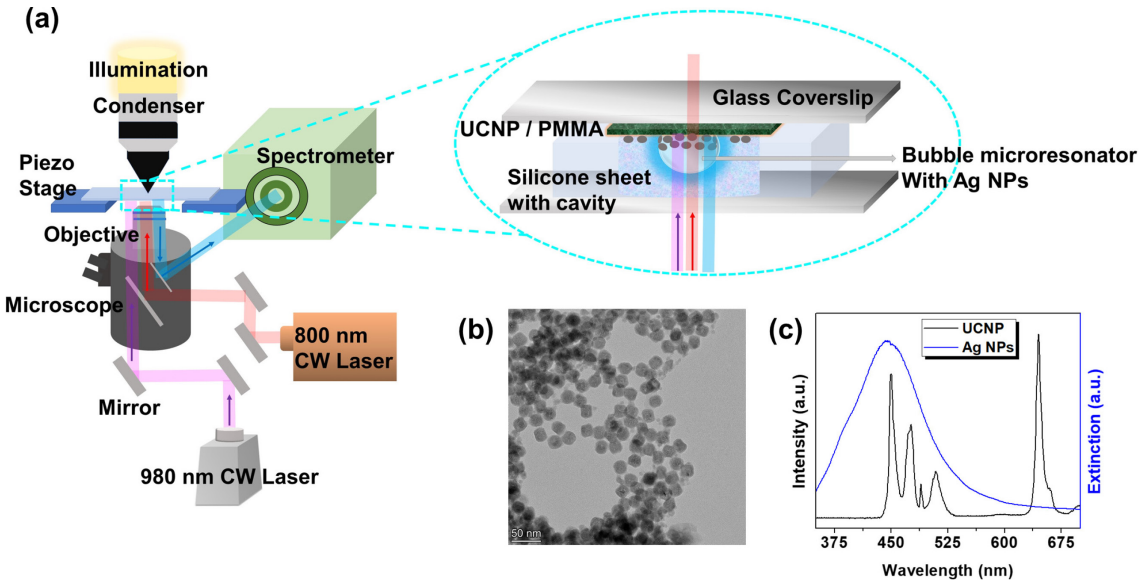


**Figure 1.** Optical setup and material characterizations for achieving laser-induced bubble micro-resonator. (a) Schematic of the optical setup for forming laser-induced bubbles and measuring upconversion emission spectra. (b) TEM image of the UCNPs with particles size ~24 nm. (c) Upconversion emission spectrum of UCNPs under 980 nm excitation and extinction spectrum of Ag NPs.

Based on the material properties, an approach was developed to obtain bubble micro-resonator suitable for enhancing emissions from the UCNPs. First, we performed multiple control experiments with different sample cells to study the formation of bubble micro-resonator. Figure 2a shows the schematic diagram of the sample cell SC1. The series of dark-field images in Figure 2b show a successful attempt towards bubble micro-resonator formation under increasing laser irradiance on the top surface of the sample cell. The intensity of the 800 nm laser was increased in the steps of 0.16 W/μm$^2$, 0.54 W/μm$^2$, and 0.8 W/μm$^2$ with corresponding exposure time of 20 seconds, 30 seconds, and 60 seconds at each step. The gradual increase in power density of 800 nm laser and corresponding exposure time ensured a better control at bubble micro-resonator formation. The bubble micro-resonator formed in this case was due to the localized heating around Ag NPs trapped by the 800 nm laser on the glass surface *via* plasmonic optothermal effect.[36,27] The Ag NP aggregates can couple together to produce new plasmonic resonant modes close to the 800

nm laser irradiation.[37-40] The plasmonic heating raised the temperature close to the kinetic limit of superheat at roughly constant pressure,[41] leading to the evaporation of the solvent and the formation of a bubble. The temperature gradient produced around the localized plasmonic heating area, resulting in the convective flow of nanomaterials towards the microbubble due to strong Marangoni convection.[27, 42] The size of the bubble can be controlled by the irradiation time. The spherical symmetry offered by the bubble provides optical WGMs suitable for photoluminescence enhancements. Although a bubble formation was observed, the distribution of UCNPs could not be controlled in this case, making it hard to study the emission enhancement of UCNPs by the bubble micro-resonator.

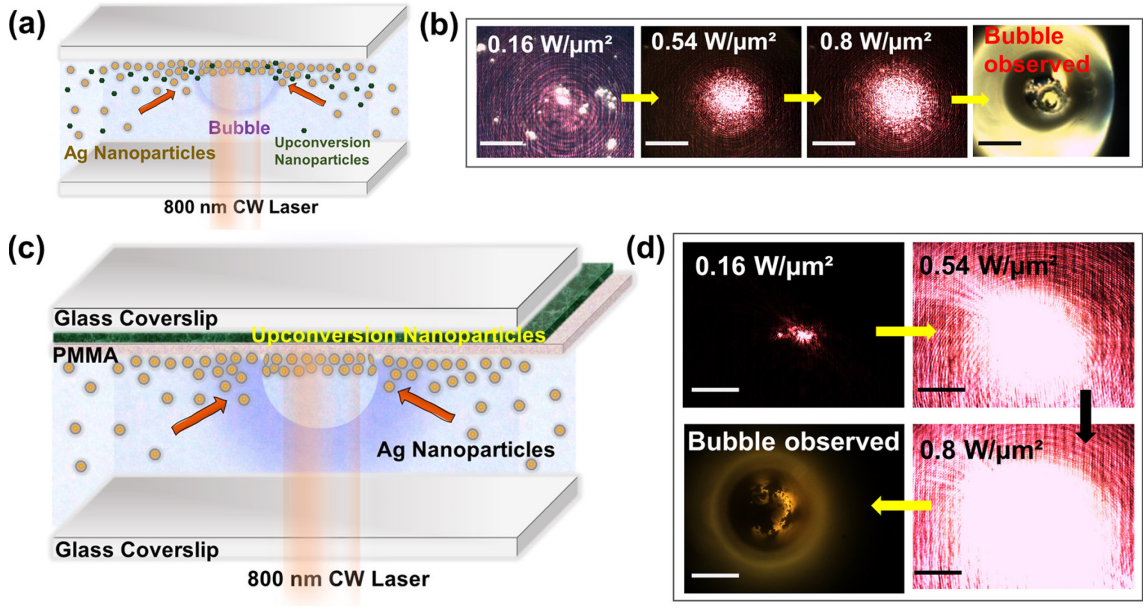


Figure 2. Formation of laser-induced bubble micro-resonator under different conditions. (a) Schematic diagram showing the sample cell SC1 comprising of a mixture of Ag NPs and UCNPs sandwiched between two glass coverslips. (b) A sequence of dark-field images showing a bubble micro-resonator formation in the corresponding sample cell under different intensities of the 800 nm laser. (c) Schematic diagram showing the sample cell SC2 comprising of Ag NPs solution beneath a bilayer thin film of PMMA/UCNPs. (d) A sequence of dark-field images showing bubble micro-resonator formation in the corresponding sample cell under different laser intensities. The scale bars are 10 μm.

To overcome this limitation, another sample cell (SC2) was designed such that UCNPs were spin coated over a glass coverslip followed by spin coating of PMMA over it. A very thin film of PMMA was coated to provide a protective layer to the UCNP film, so that the UCNPs did not come off in water and interfere with the bubble formation. The PMMA film also acted as a spacer for plasmonic enhancement of the emissions from the UCNPs due to the presence of Ag NPs. The thickness of UCNP film was about 200 nm and PMMA film was less than 10 nm as shown in Figure S5a.[43] Two control sample cells (SC3 and SC4) were also fabricated with only UCNP film in one case and Ag NPs film coated over the PMMA/UCNPs film in another case to understand the role of bubble micro-resonator in enhancing the UCNPs emissions. The spin-coated Ag NPs thin film had a thickness of about 150 nm as shown in Figure S5b. The SC2 was exposed to 800 nm laser to obtain a bubble micro-resonator over the PMMA/UCNP film as illustrated in Figure 2c. Figure 2d shows a bubble micro-resonator formation under increasing laser irradiance. The micro-resonator comprised of Ag NPs at the surface of the bubble which is at the proximity with the PMMA/UCNP film. The presence of ethylene glycol in the solution led to the formation of a more stable and durable bubble. This micro-resonator is suitable for studying the upconversion emission enhancements from the UCNP film due to the presence of Ag NPs based bubble micro-resonator. The dark-field imaging (Figure S6) and the size optimization study under laser exposure time (Figure S7) of the bubble micro-resonator is discussed in Supporting Information SIII.

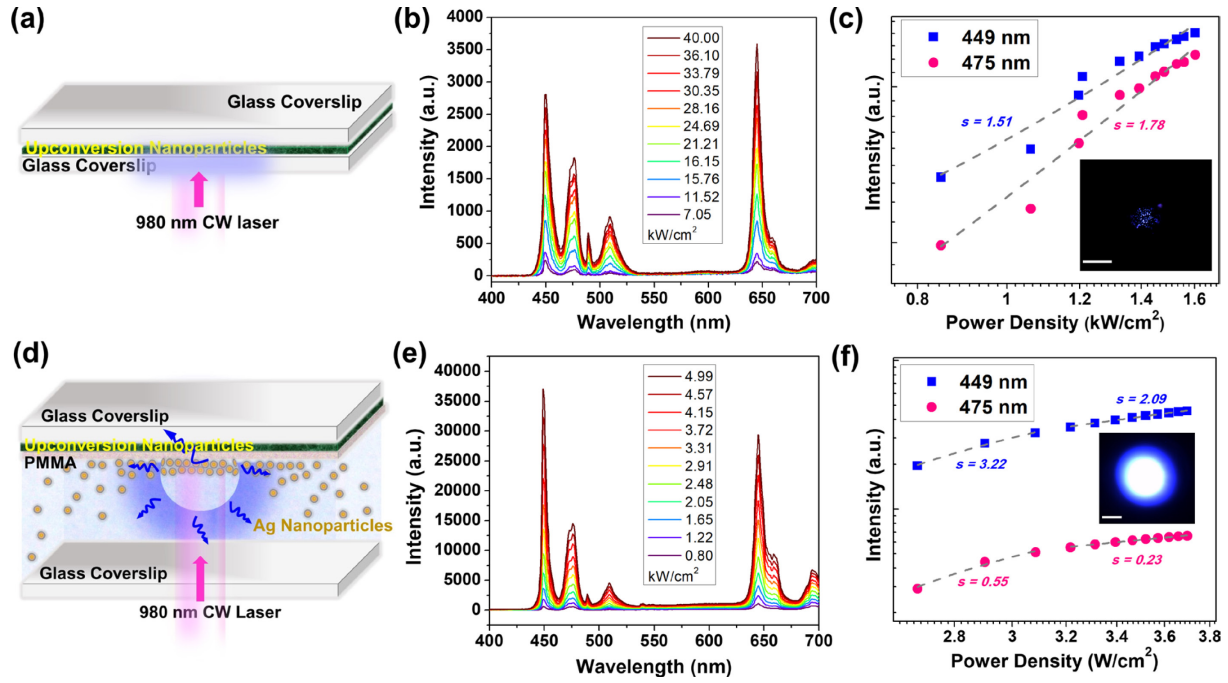


**Figure 3.** Demonstration of upconversion emission enhancement by a laser-induced bubble micro-resonator. (a) Schematic diagram of the sample cell (SC3) comprising of only UCNP film sandwiched between two glass coverslips. (b) The corresponding upconversion emission spectra of UCNP film under different laser excitation intensities. (c) The corresponding emission intensities at 449 nm and 475 nm as a function of excitation intensity. Inset: Optical image of weak blue emission under 980 nm excitation. (d) Schematic diagram of the sample cell (SC2) comprising of Ag NPs (dispersed in water and ethylene glycol) and a bubble micro-resonator formed beneath the thin films of PMMA/UCNPs. (e) The corresponding upconversion emission spectra of the PMMA/UCNP film in conjugation with Ag NPs and a bubble micro-resonator under different laser excitation intensities. (f) The corresponding emission intensities at 449 nm and 475 nm as a function of excitation intensity. Inset: Optical image of intense blue emission over the bubble micro-resonator. The scale bars are 10 μm.

A systematic study of the upconversion emissions was conducted to demonstrate the role of laser-induced bubble micro-resonator in upconversion emission enhancement. First, a control sample cell (SC3) was prepared such that a thin film of only UCNPs was spin coated over a glass coverslip with thickness of about 200 nm and sandwiched with another coverslip as illustrated in Figure 3a. Figure 3b shows the upconversion emission spectra of the UCNP film under different excitation intensities of 980 nm laser excitation. The UCNP film clearly emits in the blue and red region of the visible spectrum. The emitted wavelengths mainly include 449 nm, 474 nm, and 645 nm. The spectra show that at lower power densities of 980 nm excitation, the blue emissions were

equivalent to red emissions. This was due to subsequent lesser non-radiative relaxation of charge carriers at lower power densities in comparison to higher power densities of 980 nm laser excitation. As the excitation intensities were increased, the emissions corresponding to 645 nm starts to dominate in the emission spectra as the excited state absorption processes were suppressed and non-radiative relaxation processes dominated, resulting in two-photon excitation processes leading to prominent red emissions.[44] In general, for studying the pump power dependence of UCNPs, the emissions intensity ($I$) is related to the pump power ($P$) of the incident radiation as ($I \alpha P^n$) where n is the number of pump photons involved in the upconversion emission processes from the UCNPs. Therefore, the number of pump photons can be calculated by plotting log$P$ versus log$I$ where the slope value would give the value of n.[44] Figure 3c shows the emission intensities at 449 nm and 475 nm as a function of excitation intensity of 980 nm laser, and the inset shows an optical image of the blue emissions. The emission intensity increases with the increasing excitation intensities for both wavelengths.[45] The role of Ag NPs film in improving the upconversion emissions from UCNPs film alone in the absence of a bubble micro-resonator is further studied using a sample cell (SC4) (see Supporting Information SIV). The Ag NPs/UCNPs film helps enhance the blue emissions which is the subject of our interest.

Second, a layer of PMMA spacer was added between the Ag NPs/UCNPs film in the sample cell (SC5) as illustrated in Figure S9a. The PMMA spacer-based sample cell outperforms the upconversion emissions in comparison to the one without a PMMA spacer as discussed in Supporting Information SV. Figure 3d shows the schematic diagram of SC2 with a PMMA/ UCNP thin film and Ag NP solution under 980 nm laser excitation. The bubble attracted Ag NPs to its surface and acted as a micro-resonator for the emitted photons especially the blue emissions due to surface plasmonic resonances offered by Ag NPs. The spectra in Figure 3e clearly show that the

bubble micro-resonator along with Ag NPs can enhance the blue emissions under 980 nm laser excitation. The emitted photons are guided into the bubble micro-resonator and are totally internally reflected before resulting in an amplification of photons emitted out of the bubble micro-resonator.[46-48] The excited state absorption becomes dominant than the ground state absorption, resulting in an energy looping extinction mechanism. The emitted photons are then further totally internally reflected and are emitted as amplification of photons. At higher excitation intensities, the blue emission dominates despite higher non-radiative relaxation of charge carriers happening in the UCNP film responsible for higher red emissions. The emissions corresponding to 645 nm are also increased with increasing excitation intensities but not more than the blue emissions especially the 449 nm emissions. The emission spectra shown in Figure 3e are different from the ones shown in Figure 3b in terms of the full-width half maximum (FWHM) of the emitted spectra and the intensity ratios for different wavelengths. The FWHM is narrower for the 449 nm emissions due to the surface plasmon resonance offered by Ag NPs in comparison to other wavelengths in the emitted spectra and the emitted spectra from the only UCNP film. Figure 3f shows the corresponding emission intensity as a function of excitation intensity, and the inset shows an optical image of intense blue emissions. The upconversion emissions increase at higher excitation intensities with two different slopes for each wavelength as shown by the two linear fits. In the lower excitation regime, the slope values are higher. It is observed that under lower excitation power densities, the intensities corresponding to 449 nm and 475 nm are almost comparable. However, at higher power densities of excitation the 449 nm emissions outperform the 475 nm emissions. The slope values corresponding to 449 nm are higher than that of 475 nm both in lower and higher excitation regime. The slope values give the idea about the approximate number of NIR pump photons involved in the upconversion process. A higher slope value in the

lower power excitation corresponds to higher enhancements in comparison to higher excitation regimes. Also, a lower slope value at higher excitations corresponds to saturation of the excited states. [44, 49-51] The fact that two different slope values the emission intensity are observed for a single emitted wavelength confirms the role of bubble micro-resonator with Ag NPs. The total internal reflection of emitted photons into the bubble micro-resonator is more significant at lower excitation intensities in comparison to higher excitation intensities. Without a bubble micro-resonator, the excitation intensity of the laser is below the saturation threshold, so we only see a single slope. With a bubble micro-resonator, the upconversion emissions are eventually saturated by enhancement from the whispering gallery modes, so two different slopes will appear. This can be clearly seen in terms of the intensity ratio difference for the multiple emitted photons corresponding to different photons.

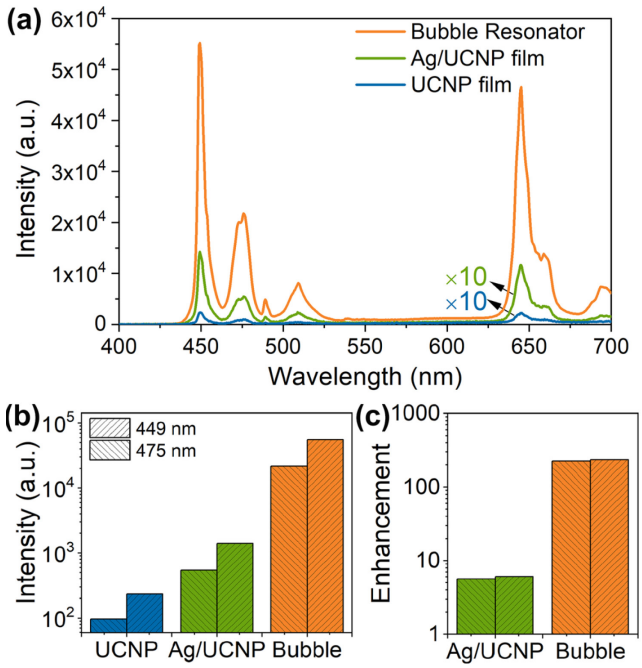


**Figure 4.** Comparison of upconversion emission enhancement from the UCNP film with and without laser-induced bubble micro-resonator. (a) Upconversion emission spectra of a UCNP film (SC3), a Ag NPs/UCNP film (SC4), and a bubble micro-resonator decorated with Ag NPs over a PMMA/UCNP film (SC2) under 7.05 kW/cm$^2$ of 980 nm laser excitation. (b) Comparison of the emission intensities at 449 nm

and 475 for the three samples. (c) Emission enhancement factor for the bubble micro-resonator (SC2) and Ag NPs/UCNP film (SC4) samples in comparison to the UCNP film.

Based on the results obtained from different sample cells mentioned above, a comparative study of the upconversion emissions from the UCNP film in the presence and absence of laser-induced bubble-micro-resonator was performed. Figure 4a shows the upconversion emission spectra of only UCNP film (SC3), Ag NPs/UCNP film (SC4), and PMMA/UCNP film in conjugation with Ag NPs and bubble micro-resonator (SC2) under 7.05 kW/cm$^2$ of 980 nm laser excitation. The upconversion emission is enhanced for UCNP film when integrated with the Ag NPs and further improved in the presence of bubble micro-resonator. The difference in the intensity values can also be clearly observed, which confirms the role of each component in the sample cell (SC2) shown in Figure 3d. Figure 4b compares the maximum emission intensities at $\lambda$ = 449 nm and 475 nm for the three cases, and Figure 4c shows the emissions enhancement factors in comparison to only UCNP film (SC3). The upconversion emissions for the sample with Ag NPs and bubble micro-resonator (SC2) were enhanced by 235 times at 449 nm and 224 times at 475 nm in comparison to the only UCNP film (SC3), while the enhancement is only 5 to 6 times for the Ag NPs/UCNP film (SC4). Furthermore, it was observed that the bubble disintegrates after a span of time leaving behind Ag NPs over the PMMA/UCNP film (SC2). The upconversion emission spectra was recorded from the UCNP film (SC2) after the bubble disintegrates to better understand and confirm the role of bubble micro-resonator for upconversion emission enhancement as discussed in Supporting Information SVI. The bubble disintegration leaves behind Ag NPs over a UCNP film (SC2) as a nearly uniform film. The emission results for the same are comparative to the Ag NPs/UCNP film (SC4).

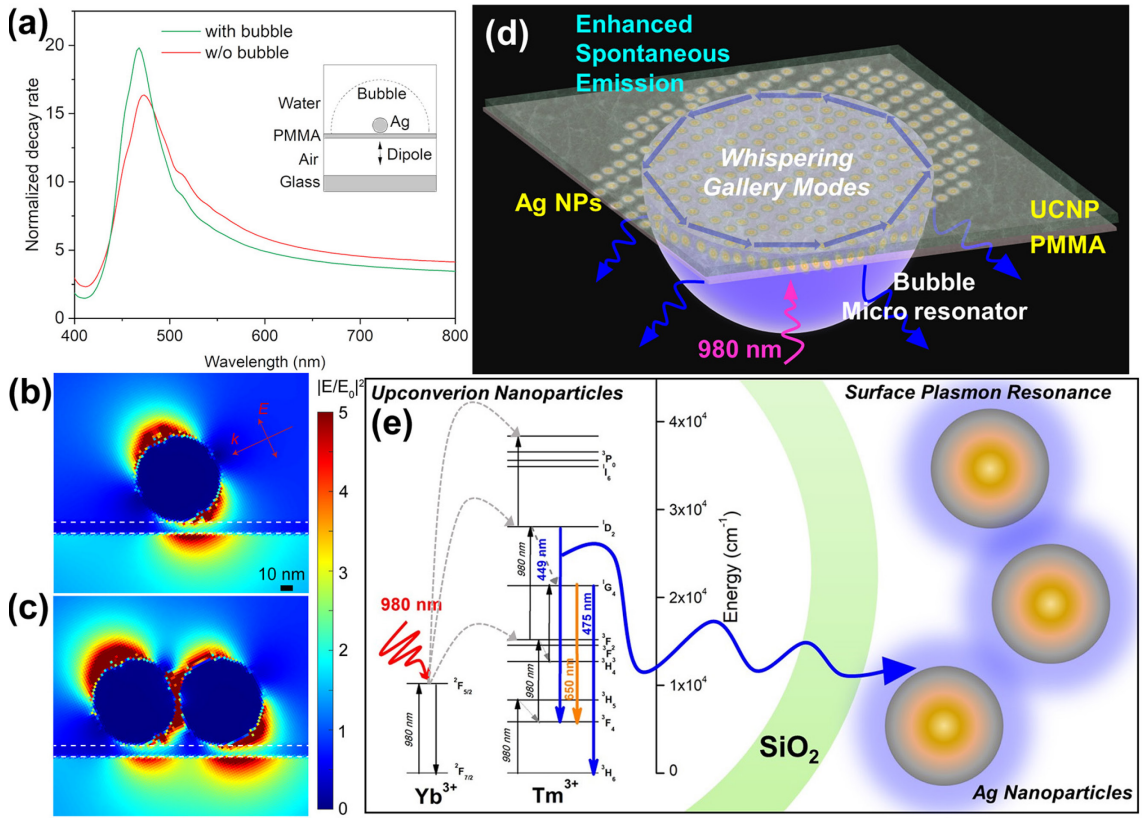


**Figure 5.** Upconversion emission mechanism and simulated luminescence enhancement of quantum emitters (UCNPs) by Ag NPs. (a) Enhancement of the emission rate of an emitter by an Ag NP antenna with and without a bubble. The radiative decay rates are normalized by that of the emitter without the antenna. The inset illustrates the FDTD simulation model. (b) Intensity of electric field around a single plasmonic Ag NP and (c) a dimer of Ag NPs separated by 2 nm. The NPs are illuminated by 980 nm light at a 64.5 deg incident angle, corresponding to the NA 1.2 of the objective. (d) Schematic diagram to show the total-internal reflection of the upconverted emitted photons and the possibility of WGMs in the bubble micro-resonator formed beneath the PMMA/UCNP film leading to spontaneous upconversion emissions enhancement. (e) Schematic energy level diagram of the core-shell UCNP comprising of $Tm^{3+}$ and $Yb^{3+}$ as dopant ions in the $NaYF_4$ host lattice (core) and $SiO_2$ (shell) showing the upconversion emissions (blue and orange dark lines) *via* combination of excited state absorption (black lines) and non-radiative relaxation transitions (grey lines) upon 980 nm laser excitation. The blue upconverted emissions have a surface plasmon resonance overlap with the Ag NPs which leads to upconversion emission enhancement.

To understand the mechanism for enhanced upconversion emissions from the UCNP film in the presence of the Ag NPs based bubble micro-resonator, we performed FDTD simulations (see Methods). In the FDTD simulation model (illustrated in the inset of Figure 5a), a dipole source is

located at 15 nm below a PMMA layer of 10 nm thickness. A glass substrate is at 200 nm below the PMMA layer, and a 70 nm diameter Ag NP is on the PMMA layer right above the dipole source. The dipole is in an air environment and the Ag NP is in water. For the simulation with a bubble, the bubble diameter is 600 nm, and we assume the Ag NP is wrapped in a water layer considering the experimental condition. Figure 5a shows that the Ag NP can enhance the radiative emission above 15 times at 475 nm, and when a bubble is present, the enhancement can reach ~20 times. In literatures, the transient photoluminescence spectroscopy results shows that the decay is faster when UCNPs are put together with plasmonic structures.[20] Therefore, along with the enhancements of photoluminescence measurements, a reduction in lifetime for UCNPs carriers is expected when placed with Ag NPs.[52] The plasmonic NPs can also enhance the local field, *i.e.*, the excitation field of the UCNPs, by ~4 times as shown in Figure 5b. Aggregation of the Ag NPs does not enhance the field further because the UCNPs are far away from the gaps, and the local fields may vary as shown in Figure 5c. The NPs are illuminated by 980 nm light at a 64.5 deg incident angle in these cases, which is the maximum angle corresponding to the NA 1.2 of the objective. At normal incident angle, the enhancement is only confined near a NP surface or inside the gap of dimer. Since there is no UCNP there, no enhancement of emission will occur as shown in Figure S11. Since the objective will create incident light at different angles, the enhancement will vary between the two boundaries in the experiment. In geometric optics, the confinement of electromagnetic radiation associated with photons in microstructures with circular symmetry is studied in terms of WGMs. In such microstructures, the electromagnetic radiations are totally internally reflected from the circular surface of the microstructures resulting in minimum reflection losses. The one round trip of the electromagnetic radiation inside the microstructure with circular orientation results in resonant modes called WGMs. The trapped electromagnetic radiation

propagates around the circumference of the dome-shaped sphere equator. At each glancing incidence of the electromagnetic radiation, reflection of the electromagnetic radiation happens off the surface of the dome-shaped sphere. Figure 5d illustrates the total-internal reflection of the upconverted emitted photons and the WGMs in the bubble micro-resonator formed beneath the PMMA/UCNP film, which lead to spontaneous upconversion emission enhancement.[53] The bubble micro-resonator also allows for the confinement of excitation NIR photons, thus increasing the probability of absorption of NIR photons by the UCNP film. The emitted photons from the UCNPs must pass through the bubble micro-resonator before being detected by the spectrometer. Thus, the emitted photons also form WGMs for upconversion emission enhancements. Figure 5e shows the schematic energy level diagram of the core-shell UCNP comprising of $Tm^{3+}$ and $Yb^{3+}$ as dopant ions in the $NaYF_4$ host lattice (core) and $SiO_2$ (shell) placed in close contact with surface plasmon resonantly matched Ag NPs. The 980 nm photons are absorbed by the $Tm^{3+}$ and $Yb^{3+}$ ions *via* energy transfer upconversion (dotted curved grey lines) and excited state upconversion processes (black lines). The two or more absorption of photons *via* excited state absorption process makes the photogenerated charge carriers rise to higher and higher energy levels.[54] These experience non-radiative relaxation decays (dotted grey lines) which results in the accumulation of the majority of photons at $^1D_2$ and $^1G_4$ energy levels. The de-excitation of photons from $^1D_2$ to $^3F_4$ leads to emission of 449 nm photons (blue line), $^1G_4$ to $^3H_6$ leads to emission of 475 nm photons (blue line), and $^1G_4$ to $^3F_4$ leads to emission of 650 nm photons (orange line). The plasmonic Ag NPs, which are present at the interface of the PMMA/UCNP films and the dome-shaped bubble micro-resonator, can enhance the optical field for the 449 nm and 475 nm photons since their surface plasmon resonances match those wavelengths as shown in Figure 1c. The enhanced blue emission is further amplified by the WGMs platform offered by the bubble micro-resonator owing

to the total internal reflection of emitted photons.[55] Thus, the integration of the bubble micro-resonator and Ag NPs offers a new platform for enhancing the blue emissions of UCNPs upon near-infrared excitation.

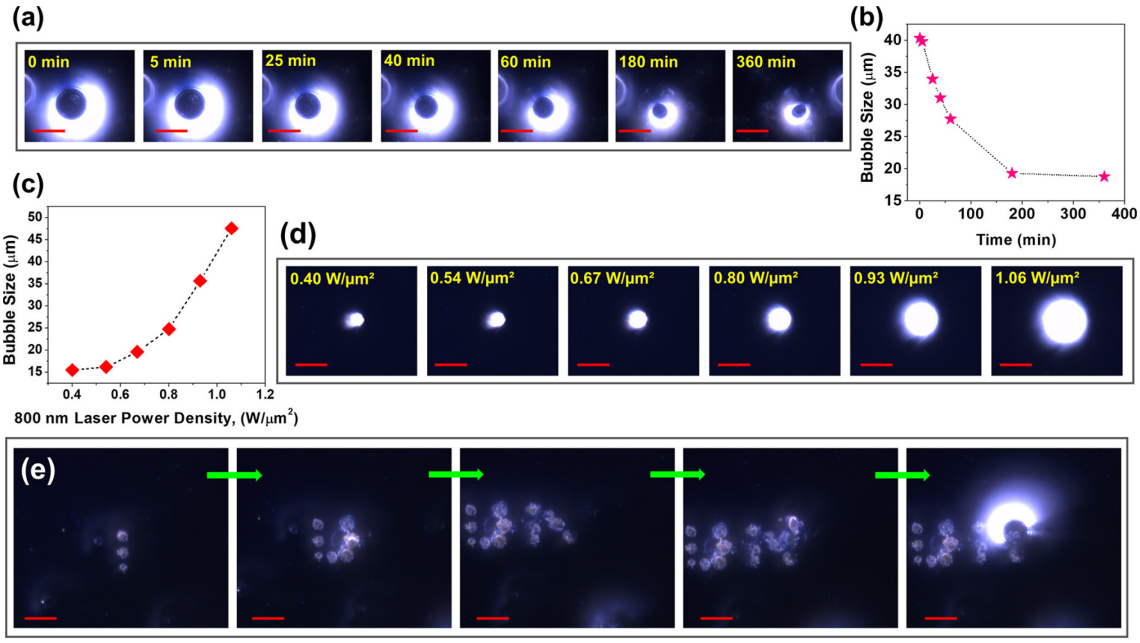


**Figure 6.** Stability test and microbubble-based lithography. (a) Dark-field images of the bubble micro-resonator shrinking in size with increasing times. (b) Bubble micro-resonator size as a function of time showcasing its stability and effectiveness. (c) Bubble micro-resonator size as a function of laser power density for 800 nm laser used for inducing the bubble with laser exposure. (d) Dark-field images of the bubble micro-resonator increasing in size with increasing intensity of the 800 nm laser. (e) Dark-field images of systematically printing Ag NPs over PMMA/UCNP film (SC2) by laser-induced bubble-pen lithography. The scale bars are 40 μm.

The stability of bubble micro-resonators is an important factor for some real-time applications. Figure 6a shows the dark-field images of a bubble micro-resonator shrinking in size after 0 to 6 hours. The change of bubble diameter as a function of time is plotted in Figure 6b, showcasing its stability and effectiveness. Figure 6c shows the bubble micro-resonator size as a function of the intensity of the 800 nm laser, which was used for inducing the bubble. Higher laser powers increase the size of the bubble exponentially due to excessive plasmonic heating of the solvents around aggregates of Ag NPs.[27, 40] Figure 6d shows the dark-field images of the bubble

micro-resonator increasing in size with larger laser intensities. Additionally, when the bubble micro-resonator bursts eventually, it leaves behind the Ag NPs over the PMMA/UCNP films (SC2). The bubble micro-resonator then works well towards depositing Ag NPs over the substrate in a controlled manner, *i.e.*, laser-induced bubble-pen lithography or bubble printing.[27, 56] Figure 6e shows the dark-field images of printing Ag NPs over PMMA/UCNP film by laser-induced bubbles. The imprinting or assembling of Ag NPs onto the PMMA/UCNP films is relevant to various biological, physical and chemical applications.[42, 57]

**Conclusion**

In conclusion, we have successfully designed and demonstrated laser-induced bubble micro-resonators in Ag NP solutions over PMMA/UCNP films for upconversion emission enhancements *via* surface plasmon resonances and WGMs. The bubble micro-resonator accumulates Ag NPs at the bubble-film interface such that Ag NPs partially covered the dome-shaped circumference of the bubble micro-resonator. The upconverted emissions from the UCNP film is enhanced $10^2$-fold in conjunction with Ag NPs and a bubble micro-resonator. Additionally, the upconversion emissions from the UCNP film can be recorded at lower excitation intensities (as low as 0.8 kW/cm$^2$). This is due to the trapping and total internal reflection of both the excitation photons and the emitted photons in the bubble micro-resonator. The durability of the bubble micro-resonator is improved by the presence of ethylene glycol in the colloidal suspension of the Ag NPs in water. In addition, the shrinking of bubbles can be used to print the Ag NPs over the PMMA/UCNP film, i.e., controlled assembly of nanomaterials over substrates by bubble-pen lithography. This multifunctional bubble micro-resonator has potential applications in biologically compatible optofluidic devices and spectroscopic platforms, e.g., cavity-based sensing devices and bubble-based micro-actuators. The integration of bubble micro-resonators with plasmonic metal NPs and

multi-stacked luminescent films opens a new avenue for fabricating multifunctional devices in line with the present biomedical technological advancements.

ASSOCIATED CONTENT

**Author Information**

*Monika Kataria, Catherine Currie Duncan, Bergen Polinko Murray, Manav Bindesh Parikh, Zijie Yan**

Department of Applied Physical Sciences, University of North Carolina at Chapel Hill, Chapel Hill, North Carolina 27599, United States

*Corresponding author: Zijie Yan zijieyan@unc.edu

**Author Contributions**

Z.Y. planned and supervised the project. M.K. proposed the idea, designed, and performed all the experiments. C.C.D., B.P.M., and M.B.P. assisted the experiments. Z.Y. performed the simulations. M.K. and Z.Y. wrote the manuscript.

**Acknowledgments**

This work was financially supported by the National Science Foundation under Grant No. 2131079.

**Supporting Information.** Synthesis and particles size distribution of UCNPs, selected area electron diffraction (SAED) pattern and TEM image of UCNPs**,** high-angle annular dark-field (HAADF) imaging of UCNPs, SEM image of the Ag NPs, cross-sectional SEM image of PMMA/UCNP film and Ag NPs/PMMA/UCNP film over silicon wafer, dark-field images of a bubble micro-resonator at different focus plane, bubble size as a function of laser exposure time,

upconversion emission studies from sample cell (SC4) consisting of thin films of Ag NPs/UCNPs sandwiched between two coverslips, upconversion emission studies from sample cell (SC5) consisting of thin films of Ag NPs/PMMA/UCNPs sandwiched between two coverslips, upconversion emissions comparison with and without PMMA spacer, comparative upconversion emission spectrum of PMMA/UCNP film in conjugation with Ag NPs based bubble micro-resonator and PMMA/UCNP film in conjugation with Ag NPs after bubble micro-resonator disintegration. The Supporting Information is available free of charge on the ACS Publications website. (PDF)

## References


1. Hong, A.-R.; Kyhm, J.-H.; Kang, G.; Jang, H. S., Orthogonal R/G/B upconversion luminescence-based full-color tunable upconversion nanophosphors for transparent displays. *Nano Letters* **2021,** *21* (11), 4838-4844.
2. Bi, S.; Deng, Z.; Huang, J.; Wen, X.; Zeng, S., NIR-II Responsive Upconversion Nanoprobe with Simultaneously Enhanced Single-Band Red Luminescence and Phase/Size Control for Bioimaging and Photodynamic Therapy. *Advanced Materials* **2022**, 2207038.
3. Lin, G.; Jin, D., Responsive Sensors of Upconversion Nanoparticles. *ACS sensors* **2021,** *6* (12), 4272-4282.
4. Kataria, M.; Yadav, K.; Haider, G.; Liao, Y. M.; Liou, Y.-R.; Cai, S.-Y.; Lin, H.-i.; Chen, Y. H.; Paul Inbaraj, C. R.; Bera, K. P., Transparent, wearable, broadband, and highly sensitive upconversion nanoparticles and graphene-based hybrid photodetectors. *ACS Photonics* **2018,** *5* (6), 2336-2347.
5. Kataria, M.; Yadav, K.; Cai, S.-Y.; Liao, Y.-M.; Lin, H.-I.; Shen, T. L.; Chen, Y.-H.; Chen, Y.-T.; Wang, W.-H.; Chen, Y.-F., Highly sensitive, visible blind, wearable, and omnidirectional near-infrared photodetectors. *ACS nano* **2018,** *12* (9), 9596-9607.
6. Bi, W.; Wu, Y.; Chen, C.; Zhou, D.; Song, Z.; Li, D.; Chen, G.; Dai, Q.; Zhu, Y.; Song, H., Dye sensitization and local surface plasmon resonance-enhanced upconversion luminescence for efficient perovskite solar cells. *ACS applied materials & interfaces* **2020,** *12* (22), 24737-24746.
7. Rao, M.; Fan, C.; Ji, J.; Liang, W.; Wei, L.; Zhang, D.; Yan, Z.; Wu, W.; Yang, C., Catalytic Chiral Photochemistry Sensitized by Chiral Hosts-Grafted Upconverted Nanoparticles. *ACS Applied Materials & Interfaces* **2022**.
8. Li, M.; Zheng, Z.; Zheng, Y.; Cui, C.; Li, C.; Li, Z., Controlled growth of metal–organic framework on upconversion nanocrystals for NIR-enhanced photocatalysis. *ACS Applied Materials & Interfaces* **2017,** *9* (3), 2899-2905.

9. Liu, K.; Liu, X.; Zeng, Q.; Zhang, Y.; Tu, L.; Liu, T.; Kong, X.; Wang, Y.; Cao, F.; Lambrechts, S. A., Covalently assembled NIR nanoplatform for simultaneous fluorescence imaging and photodynamic therapy of cancer cells. *ACS nano* **2012,** *6* (5), 4054-4062.
10. Zhang, Y.; Xue, X.; Fang, M.; Pang, G.; Xing, Y.; Zhang, X.; Li, L.; Chen, Q.; Wang, Y.; Chang, J., Upconversion Optogenetic Engineered Bacteria System for Time-Resolved Imaging Diagnosis and Light-Controlled Cancer Therapy. *ACS Applied Materials & Interfaces* **2022**.
11. Li, L.; Song, M.; Lao, X.; Pang, S.-Y.; Liu, Y.; Wong, M.-C.; Ma, Y.; Yang, M.; Hao, J., Rapid and ultrasensitive detection of SARS-CoV-2 spike protein based on upconversion luminescence biosensor for COVID-19 point-of-care diagnostics. *Materials & Design* **2022**, 111263.
12. Zhang, H.; Zhang, H., Rare earth luminescent materials. Nature Publishing Group: 2022; Vol. 11, pp 1-3.
13. Liao, J.; Wang, M.; Lin, F.; Han, Z.; Fu, B.; Tu, D.; Chen, X.; Qiu, B.; Wen, H.-R., Thermally boosted upconversion and downshifting luminescence in Sc2 (MoO4) 3: Yb/Er with two-dimensional negative thermal expansion. *Nature communications* **2022,** *13* (1), 1-11.
14. Jiang, B.; Zhu, S.; Wang, W.; Li, J.; Dong, C.-H.; Shi, L.; Zhang, X., Room-temperature Continuous-Wave Upconversion White Microlaser Using a Rare-earth-Doped Microcavity. *ACS Photonics* **2022,** *9* (9), 2956-2962.
15. Xie, X.; Li, Q.; Chen, H.; Wang, W.; Wu, F.; Tu, L.; Zhang, Y.; Kong, X.; Chang, Y., Manipulating the Injected Energy Flux via Host-Sensitized Nanostructure for Improving Multiphoton Upconversion Luminescence of Tm3+. *Nano Letters* **2022,** *22* (13), 5339-5347.
16. Wen, S.; Zhou, J.; Zheng, K.; Bednarkiewicz, A.; Liu, X.; Jin, D., Advances in highly doped upconversion nanoparticles. *Nature communications* **2018,** *9* (1), 1-12.
17. Lin, H.-I.; Yadav, K.; Shen, K.-C.; Haider, G.; Roy, P. K.; Kataria, M.; Chang, T.-J.; Li, Y.-H.; Lin, T.-Y.; Chen, Y.-T., Nanoscale Core–Shell Hyperbolic Structures for Ultralow Threshold Laser Action: An Efficient Platform for the Enhancement of Optical Manipulation. *ACS applied materials & interfaces* **2018,** *11* (1), 1163-1173.
18. Lin, H.-I.; Tan, H.-Y.; Liao, Y.-M.; Shen, K.-C.; Shalaginov, M. Y.; Kataria, M.; Chen, C.-T.; Chang, J.-W.; Chen, Y.-F., A Transferrable, Adaptable, Free-Standing, and Water-Resistant Hyperbolic Metamaterial. *ACS Applied Materials & Interfaces* **2021,** *13* (41), 49224-49231.
19. Lin, H.-I.; Wang, C.-C.; Shen, K.-C.; Shalaginov, M. Y.; Roy, P. K.; Bera, K. P.; Kataria, M.; Paul Inbaraj, C. R.; Chen, Y.-F., Enhanced laser action from smart fabrics made with rollable hyperbolic metamaterials. *npj Flexible Electronics* **2020,** *4* (1), 1-10.
20. Das, A.; Mao, C.; Cho, S.; Kim, K.; Park, W., Over 1000-fold enhancement of upconversion luminescence using water-dispersible metal-insulator-metal nanostructures. *Nature communications* **2018,** *9* (1), 1-11.
21. Chen, H.; Jiang, Z.; Hu, H.; Kang, B.; Zhang, B.; Mi, X.; Guo, L.; Zhang, C.; Li, J.; Lu, J., Sub-50-ns ultrafast upconversion luminescence of a rare-earth-doped nanoparticle. *Nature Photonics* **2022,** *16* (9), 651-657.
22. Guo, Q.; Zhang, J.; Ning, C.; Zhuo, N.; Zhai, S.; Liu, J.; Wang, L.; Liu, S.; Jia, Z.; Liu, F., Continuous-Wave Operation of Microcavity Quantum Cascade Lasers in Whispering-Gallery Mode. *ACS Photonics* **2022,** *9* (4), 1172-1179.
23. Yan, Y.; He, J.; Wang, M.; Yang, L.; Jiang, Y., Microsphere Photonic Superlens for a Highly Emissive Flexible Upconversion-Nanoparticle-Embedded Film. *ACS Applied Materials & Interfaces* **2022**.

24. Sato, R.; Henzie, J.; Zhang, B.; Ishii, S.; Murai, S.; Takazawa, K.; Takeda, Y., Random Lasing via Plasmon-Induced Cavitation of Microbubbles. *Nano Letters* **2021,** *21* (14), 6064-6070.
25. Aliannezhadi, M.; Mozaffari, M. H.; Amirjan, F., Optofluidic R6G microbubble DBR laser: A miniaturized device for highly sensitive lab-on-a-chip biosensing. *Photonics and Nanostructures-Fundamentals and Applications* **2023,** *53*, 101108.
26. Giannetti, A.; Barucci, A.; Berneschi, S.; Cosci, A.; Cosi, F.; Farnesi, D.; Conti, G. N.; Pelli, S.; Soria, S.; Tombelli, S. In *Optical micro-bubble resonators as promising biosensors*, Optical Sensors 2015, SPIE: 2015; pp 241-247.
27. Kollipara, P. S.; Mahendra, R.; Li, J.; Zheng, Y., Bubble-pen lithography: Fundamentals and applications. *Aggregate* **2022**, e189.
28. Kim, H.; Youn, S.; Kim, J.; Park, S.; Lee, M.; Hwang, J. Y.; Chang, J. H., Deep laser microscopy using optical clearing by ultrasound-induced gas bubbles. *Nature Photonics* **2022**, 1-7.
29. Harley, W. S.; Kolesnik, K.; Xu, M.; Heath, D. E.; Collins, D. J., 3D Acoustofluidics via Sub-Wavelength Micro-Resonators. *Advanced Functional Materials* **2022**, 2211422.
30. Liao, J.; Qavi, A. J.; Adolphson, M. R.; Yang, L. In *Packaged microbubble resonators as a robust biosensing device*, Frontiers in Biological Detection: From Nanosensors to Systems XIV, SPIE: 2022; p 1197902.
31. Sun, L.; Lehnert, T.; Li, S.; Gijs, M. A., Bubble-enhanced ultrasonic microfluidic chip for rapid DNA fragmentation. *Lab on a Chip* **2022,** *22* (3), 560-572.
32. Yadav, K.; Chou, A.-C.; Ulaganathan, R. K.; Gao, H.-D.; Lee, H.-M.; Pan, C.-Y.; Chen, Y.-T., Targeted and efficient activation of channelrhodopsins expressed in living cells via specifically-bound upconversion nanoparticles. *Nanoscale* **2017,** *9* (27), 9457-9466.
33. Bharadwaj, P.; Novotny, L., Spectral dependence of single molecule fluorescence enhancement. *Optics Express* **2007,** *15* (21), 14266-14274.
34. Novotny, L.; Hecht, B., *Principles of nano-optics*. Cambridge university press: 2012.
35. Paramelle, D.; Sadovoy, A.; Gorelik, S.; Free, P.; Hobley, J.; Fernig, D. G., A rapid method to estimate the concentration of citrate capped silver nanoparticles from UV-visible light spectra. *Analyst* **2014,** *139* (19), 4855-4861.
36. Xie, Y.; Zhao, C., An optothermally generated surface bubble and its applications. *Nanoscale* **2017,** *9* (20), 6622-6631.
37. Kinnan, M. K.; Chumanov, G., Plasmon coupling in two-dimensional arrays of silver nanoparticles: II. Effect of the particle size and interparticle distance. *The Journal of Physical Chemistry C* **2010,** *114* (16), 7496-7501.
38. Jiang, M.-M.; Chen, H.-Y.; Li, B.-H.; Liu, K.-W.; Shan, C.-X.; Shen, D.-Z., Hybrid quadrupolar resonances stimulated at short wavelengths using coupled plasmonic silver nanoparticle aggregation. *Journal of Materials Chemistry C* **2014,** *2* (1), 56-63.
39. Merkl, P.; Zhou, S.; Zaganiaris, A.; Shahata, M.; Eleftheraki, A.; Thersleff, T.; Sotiriou, G. A., Plasmonic coupling in silver nanoparticle aggregates and their polymer composite films for near-infrared photothermal biofilm eradication. *ACS applied nano materials* **2021,** *4* (5), 5330-5339.
40. Ohlinger, A.; Nedev, S.; Lutich, A. A.; Feldmann, J., Optothermal escape of plasmonically coupled silver nanoparticles from a three-dimensional optical trap. *Nano letters* **2011,** *11* (4), 1770-1774.
41. Yan, Z.; Chrisey, D. B., Pulsed laser ablation in liquid for micro-/nanostructure generation. *Journal of Photochemistry and Photobiology C: Photochemistry Reviews* **2012,** *13* (3), 204-223.

42. Hill, E. H.; Goldmann, C.; Hamon, C.; Herber, M., Laser-Driven Bubble Printing of Plasmonic Nanoparticle Assemblies onto Nonplasmonic Substrates. *The Journal of Physical Chemistry C* **2022**.
43. Li, K.; Jiang, K.; Zhang, L.; Wang, Y.; Mao, L.; Zeng, J.; Lu, Y.; Wang, P., Raman scattering enhanced within the plasmonic gap between an isolated Ag triangular nanoplate and Ag film. *Nanotechnology* **2016,** *27* (16), 165401.
44. Rai, V. K., *Upconverting Nanoparticles: From Fundamentals to Applications*. John Wiley & Sons: 2022.
45. Liu, K.; Wang, Y.; Kong, X.; Liu, X.; Zhang, Y.; Tu, L.; Ding, Y.; Aalders, M. C.; Buma, W. J.; Zhang, H., Multispectral upconversion luminescence intensity ratios for ascertaining the tissue imaging depth. *Nanoscale* **2014,** *6* (15), 9257-9263.
46. Fernandez-Bravo, A.; Yao, K.; Barnard, E. S.; Borys, N. J.; Levy, E. S.; Tian, B.; Tajon, C. A.; Moretti, L.; Altoe, M. V.; Aloni, S., Continuous-wave upconverting nanoparticle microlasers. *Nature nanotechnology* **2018,** *13* (7), 572-577.
47. Bednarkiewicz, A.; Chan, E. M.; Kotulska, A.; Marciniak, L.; Prorok, K., Photon avalanche in lanthanide doped nanoparticles for biomedical applications: super-resolution imaging. *Nanoscale Horizons* **2019,** *4* (4), 881-889.
48. Malhotra, K.; Hrovat, D.; Kumar, B.; Qu, G.; Houten, J. V.; Ahmed, R.; Piunno, P. A.; Gunning, P. T.; Krull, U. J., Lanthanide-Doped Upconversion Nanoparticles: Exploring A Treasure Trove of NIR-Mediated Emerging Applications. *ACS Applied Materials & Interfaces* **2023**.
49. Das, A.; Mao, C.; Cho, S.; Kim, K.; Park, W., Over 1000-fold enhancement of upconversion luminescence using water-dispersible metal-insulator-metal nanostructures. *Nature communications* **2018,** *9* (1), 4828.
50. Ahn, I. H.; Yeo, S. J.; Jung, K.; Kang, G.; Shin, D. H.; Jang, H. S.; Kim, B.; Nam, M.; Kwon, S. J.; Ko, D. H., A multi-functional highly efficient upconversion luminescent film with an array of dielectric microbeads decorated with metal nanoparticles. *Advanced Functional Materials* **2020,** *30* (13), 1909445.
51. Fernandez-Bravo, A.; Wang, D.; Barnard, E. S.; Teitelboim, A.; Tajon, C.; Guan, J.; Schatz, G. C.; Cohen, B. E.; Chan, E. M.; Schuck, P. J., Ultralow-threshold, continuous-wave upconverting lasing from subwavelength plasmons. *Nature materials* **2019,** *18* (11), 1172-1176.
52. Kataria, M.; Yadav, K.; Nain, A.; Lin, H.-I.; Hu, H.-W.; Paul Inbaraj, C. R.; Chang, T.-J.; Liao, Y.-M.; Cheng, H.-Y.; Lin, K.-H., Self-sufficient and highly efficient gold sandwich upconversion nanocomposite lasers for stretchable and bio-applications. *ACS applied materials & interfaces* **2020,** *12* (17), 19840-19854.
53. Hu, H.-W.; Haider, G.; Liao, Y.-M.; Roy, P. K.; Lin, H.-I.; Lin, S.-Y.; Chen, Y.-F., Ultralow Threshold Cavity-Free Laser Induced by Total Internal Reflection. *ACS omega* **2020,** *5* (30), 18551-18556.
54. Pattnaik, S.; Mondal, M.; Mukhopadhyay, L.; Basak, S.; Rai, V. K.; Giri, R.; Singh, V., Frequency upconversion based thermally stable molybdate phosphors in a temperature sensing probe. *New Journal of Chemistry* **2022**.
55. Barannik, A. A.; Bunyaev, S. A.; Cherpak, N. T.; Prokopenko, Y. V.; Kharchenko, A. A.; Vitusevich, S. A., Whispering gallery mode hemisphere dielectric resonators with impedance plane. *IEEE transactions on microwave theory and techniques* **2010,** *58* (10), 2682-2691.

56. Lin, L.; Peng, X.; Mao, Z.; Li, W.; Yogeesh, M. N.; Rajeeva, B. B.; Perillo, E. P.; Dunn, A. K.; Akinwande, D.; Zheng, Y., Bubble-pen lithography. *Nano letters* **2016,** *16* (1), 701-708.
57. Bao, Y.; Yan, Z.; Scherer, N. F., Optical printing of electrodynamically coupled metallic nanoparticle arrays. *The Journal of Physical Chemistry C* **2014,** *118* (33), 19315-19321.

**For Table of Contents Use only**